

Combined Field and Circuit Theories in Squirrel-Cage Induction Motors Based on Micro-T Circuit Model

L. Qaseer, F. de León, and S. Purushothaman

Department of Electrical and Computer Engineering
Polytechnic Institute of New York University, Brooklyn, NY 11417, USA
lqaseer@poly.edu, fdeleon@poly.edu, sujitp@ieee.org

Abstract — This paper presents an equivalent circuit derived directly from Maxwell's equations in a manner to show the amalgamation of field models and the circuit theory. A micro-T equivalent circuit is obtained from the solution of Maxwell's equations for a cylindrical representation of a squirrel cage induction motor. First, a general form of the field solution is obtained using transfer matrices. A variable transformation is then applied, which makes it possible to derive a circuit for each annular region in the motor. By joining the equivalent circuits in cascade, a complete equivalent circuit for the motor is obtained. The voltages and currents in the equivalent circuit relate directly to the field quantities within the actual motor. Accuracy of the method is verified with comparisons against finite elements and a commercial motor design program.

Index Terms — Eddy currents, electromagnetic induction, equivalent circuits, induction motors.

I. INTRODUCTION

Multiregion traveling wave problems in electrical machines have been treated in detail by a number of authors; see for example [1-11]. A traveling wave is usually produced by a polyphase winding, which acts upon a series of laminar regions. A region is defined, for the purposes of this paper, as an area in the motor in which the material is uniform in nature, having boundaries of

simple cylindrical shape. When any of the regions is conducting, eddy currents are induced and forces tangential to the plane of the region are established. If the field quantities at the region interfaces are known, these forces can be calculated. Typical problems include linear induction motors [1], rotating induction motors [2-5], drag-cup servomotors [6], liquid metal induction pumps and generators [7], and armature reaction losses in solid poles [8-11].

The theory of induction motors is usually presented in one of two ways: either the motor is represented by a Steinmetz equivalent circuit [12], or analytical expressions are derived from the electromagnetic field theory [2-4], [13]. As of yet there is no general method enabling one to derive an equivalent circuit directly from a field solution. Of course, it is always possible to set up an analogue model of differential equations [14], but the number of elements required for accurate modeling can be very large.

As the number of regions is increased, the algebraic complexity of the field solution becomes prone to errors. Additionally, if the motor model is altered by adding extra regions, it is necessary to repeat the complete field analysis. The micro-T equivalent circuits developed in this paper have the form of cascaded transmission lines; therefore, it is possible to consider any number of regions without recurring to lengthy analyses. The micro-T circuit offers a direct relationship between field quantities in the motor voltages and currents in the equivalent circuit (see Fig. 1).

The use of an equivalent circuit can give deep

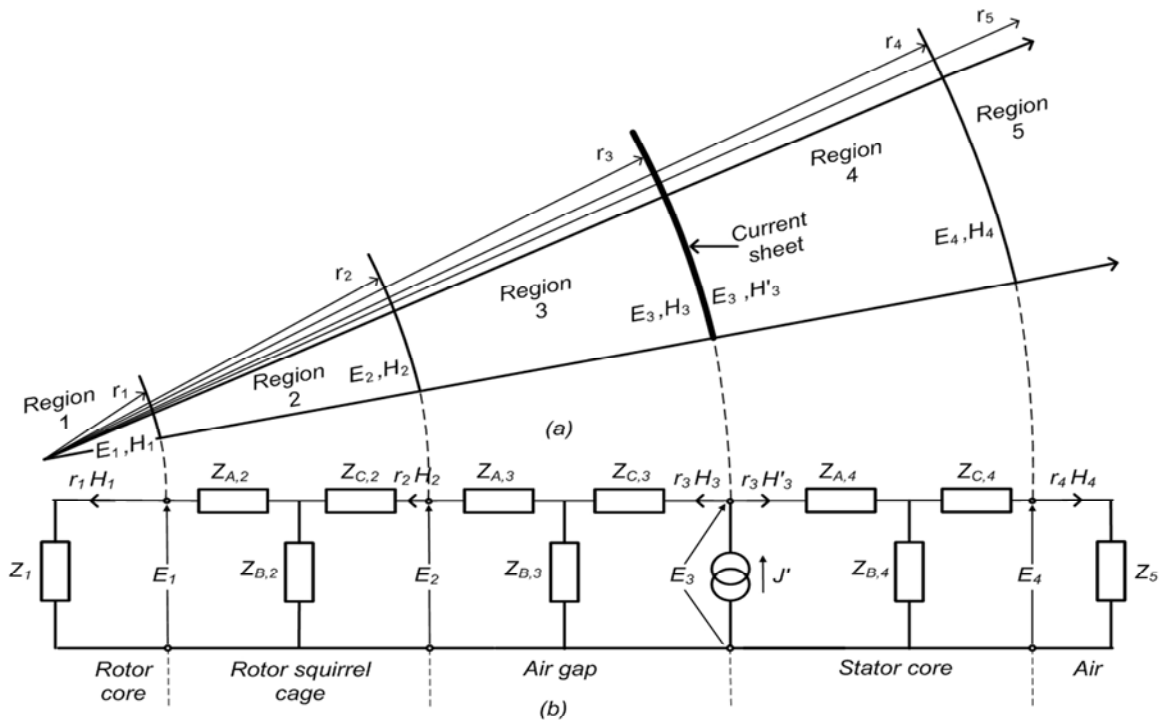


Fig.1. (a) Cross-sectional sextant through a multi-layer squirrel cage induction motor. (b) Basic equivalent circuit for a five-region squirrel cage induction motor.

insight into the behavior of the motor. Engineers are trained to interpret equivalent circuits, and once the circuit elements have been obtained, the amount of calculations required for a given set of conditions is relatively small. The motor model can be made more detailed when adding extra regions by inserting extra terms in the equivalent circuit at the appropriate points.

The combination of field and circuit theories has been used in other areas; see for example [15 and 16]. In [15], a hybrid electromagnetic-circuit is used for the simulation of microwave devices together with nonlinear lumped circuits. A circuit-oriented, finite-element solution is proposed in [16] to analyze travelling wave coupled problems. The micro-T circuit theory has been used in [17] and [18] to analyze induction heating problems.

The contributions of this paper are: the application of the micro-T theory to the solution of the electromagnetic field distribution in squirrel cage induction motors; the derivation of a terminal equivalent circuit from the solution of Maxwell's equations in the motor.

The equivalent circuit of this paper gives information not only on the terminal performance of the motor, but allows looking at the behavior of the electromagnetic field in the different layers.

The accuracy of the method has been verified with finite elements simulations and with the equivalent circuit on a real motor.

II. MATHEMATICAL MODEL

A general multiregion problem is analyzed. Figure 1a shows a sextant of a motor comprising of $N (=5)$ concentric cylinders. The excitation is an infinitesimally thin and axially infinite current sheet at radius r_g . It is further assumed that displacement currents and magnetic saturation are negligible.

Three field quantities which are acting at the region boundaries will be considered in this analysis. These are the electric field strength E which is directed axially along the interface, the magnetic field strength H which is directed circumferentially along the interface, and the third one is the flux density B normal to the interface in the radial direction. The analysis using these field components is performed to obtain field quantities at the region boundaries. After these field quantities are known, the equivalent circuit is then derived and the power flow through the interfaces, torque, output power, rotor losses, and rotational force are obtained.

The intermediate stage between the field

solution and the final equivalent circuit is represented in a transmission line form [17]. The E and H values on either side of a region are linked by a transfer matrix [19-20]. Therefore each bounded region in the model shown in Fig. 1 can be represented by a corresponding transfer matrix equation.

The circuit model of this paper is derived from the analytical solution of Maxwell's equations. The following geometrical simplifications have been made: (1) the stator windings (including slots and teeth) have been substituted by a current sheet; (2) the squirrel cage has been substituted by a conductive equivalent layer. The first assumption prevents the accurate representation of the stator winding resistance while the second assumption produces a larger than normal magnetizing current. Both limitations can be potentially eliminated with the use of homogenous equivalent media [20]. This, however, is beyond the scope of this paper, but we intend to continue our research in that direction.

III. THEORETICAL ANALYSIS

A. Field theory solution of a general region

It is assumed that the winding produces a perfect sinusoidal traveling wave. The line current density may be represented as

$$J_z = \text{Re} \left\{ \hat{J} e^{j(\omega t - p\phi)} \right\} \quad (1)$$

where \hat{J} , ω and p are the amplitude of line current density, angular frequency, and the number of pole pairs. The field produced will link all cylindrical regions from 1 to N . Maxwell's equations are solved accordingly. As a first step in the analysis, the field components of a general region are derived, assuming that all fields vary as $\exp(\omega t - p\phi)$, and omitting this factor from all field expressions that follow (we work only with the amplitudes of the travelling wave functions). Then, Maxwell's equations for any region in the model are:

$$\nabla \times \hat{H} = \hat{J}, \quad (2)$$

$$\nabla \times \hat{E} = -j\omega \hat{B}, \quad (3)$$

with

$$\hat{J} = \sigma \hat{E}, \quad (4)$$

and

$$\hat{B} = \mu \hat{H}. \quad (5)$$

The boundary conditions are

- 1) The radial component of the flux density is continuous across a boundary.
- 2) The circumferential component of magnetic field strength is continuous across a boundary, but one must consider the effects of the current sheet as shown in sub-section B.

Taking the r -component from both sides of (3) yields

$$E_z = \frac{\omega}{p} (r B_r), \quad (6)$$

and taking only the Φ -component from both sides of (3) yields

$$\frac{\partial E_z}{\partial r} = j\omega \mu H_\phi. \quad (7)$$

Using (2) and (4) and taking the z -component from both sides gives

$$\sigma E_z = \frac{1}{r} \frac{\partial}{\partial r} (r H_\phi) + j \frac{p}{r} H_r. \quad (8)$$

Equation (8) can be written, after rearranging, in the following form

$$r^2 \frac{\partial^2 E_z}{\partial r^2} + r \frac{\partial E_z}{\partial r} - (\alpha^2 r^2 + p^2) E_z = 0. \quad (9)$$

The solution is given by

$$E_z = C_1 I_p(\alpha r) + C_2 K_p(\alpha r), \quad (10)$$

where I_p and K_p are the modified Bessel functions of order p and of general complex argument, C_1 and C_2 are constants to be evaluated from boundary conditions, and $\alpha^2 = j\omega\mu\sigma$ where μ and σ represent the absolute permeability and conductivity and ω is replaced by $s\omega$ in the above equation for a region moving with slip s .

From (3), (5), and (10) we have

$$H_\phi = \frac{\alpha}{j\omega\mu} [C_1 I'_p(\alpha r) + C_2 K'_p(\alpha r)]. \quad (11)$$

For non-conducting regions or regions moving at synchronous speed, the governing partial differential equation is

$$r^2 \frac{\partial^2 E_z}{\partial r^2} + r \frac{\partial E_z}{\partial r} - p^2 E_z = 0, \quad (12)$$

and the solution is given by

$$E_z = C_1 r^{-p} + C_2 r^p. \quad (13)$$

Therefore,

$$H_\phi = -\frac{p}{j\omega r \mu} (C_1 r^{-p} - C_2 r^p). \quad (14)$$

B. Field calculations at region boundaries

Figure 2a shows a general region n , where $E_{z,n}$ and $H_{\phi,n}$ are the field components at the upper boundary of region n , and $E_{z,n-1}$ and $H_{\phi,n-1}$ are the equivalent values at the lower boundary of the same region. Considering a conducting region whose slip is different from zero, from (10) and (11)

$$E_{z,n} = C_1 I_p(\alpha_n r_n) + C_2 K_p(\alpha_n r_n), \quad (15)$$

$$H_{\phi,n} = \frac{\alpha_n}{j\omega\mu_n} \left[C_1 I'_p(\alpha_n r_n) + C_2 K'_p(\alpha_n r_n) \right]. \quad (16)$$

Equivalent expressions for $E_{z,n-1}$ and $H_{\phi,n-1}$ can be found by replacing r_n in the above equations by r_{n-1} . Similar argument applies for a non-conducting region using (13) and (14). Now for regions $1 < n < N$ we have:

$$\begin{bmatrix} E_{z,n} \\ H_{\phi,n} \end{bmatrix} = [T_n] \cdot \begin{bmatrix} E_{z,n-1} \\ H_{\phi,n-1} \end{bmatrix}, \quad (17)$$

where $[T_n]$ is the transfer matrix [19], [22] for region n and is given by

$$[T_n] = \begin{bmatrix} a_n & b_n \\ c_n & d_n \end{bmatrix}. \quad (18)$$

The expressions for a_n , b_n , c_n , and d_n are given in the Appendix. Knowing the values of E_z and H_ϕ at the inner boundary of a region, the values of E_z and H_ϕ at the outer boundary can be obtained from this simple transfer matrix relation. At the boundaries where no excitation current sheet exists, E_z and H_ϕ are continuous; thus for example, if two contiguous regions have no current sheet at the common boundary, knowing E_z and H_ϕ at the inner boundary of the external region, E_z and H_ϕ at the outer boundary of the inner region can be calculated by successive use of the underlying two transfer matrices. Consider that the excitation current sheet is located at radius r_g , then

$$H'_{\phi,n} = H_{\phi,n}, \quad n \neq g, \quad (19)$$

$$H'_{\phi,n} = H_{\phi,n} + J', \quad n = g, \quad (20)$$

where $H_{\phi,n}$ is the circumferential magnetic field strength in close inner proximity to the boundary and $H'_{\phi,n}$ is the circumferential magnetic field strength in close outer proximity to the boundary.

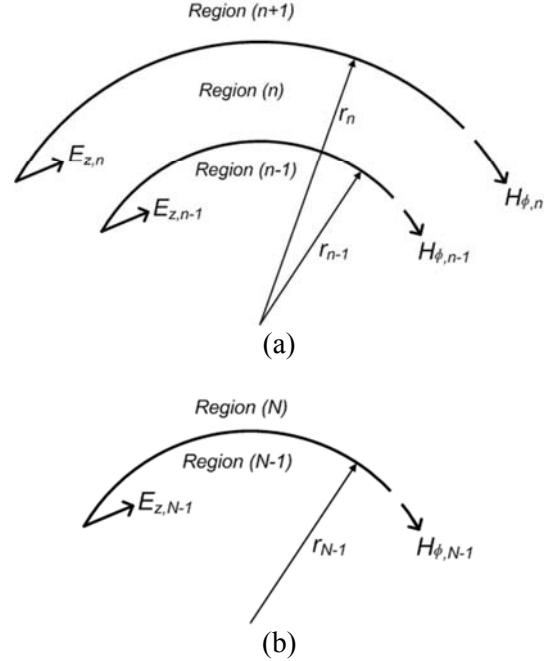


Fig. 2. Mathematical model. (a) General region n ; (b) end region N .

Bearing in mind the boundary conditions, it is apparent that for the model considered, we can write

$$\begin{bmatrix} E_{z,n-1} \\ H_{\phi,n-1} \end{bmatrix} = [T_{n-1}] \cdot [T_{n-2}] \cdots [T_{g+1}] \cdot \begin{bmatrix} E_{z,g} \\ H_{\phi,g} + J' \end{bmatrix}, \quad (21)$$

$$\begin{bmatrix} E_{z,g} \\ H_{\phi,g} \end{bmatrix} = [T_g] \cdot [T_{g-1}] \cdots [T_2] \cdot \begin{bmatrix} E_{z,1} \\ H_{\phi,1} \end{bmatrix}. \quad (22)$$

If regions 1 and N are now considered then the field should vanish for $r=0$ and $r=\infty$, hence

$$E_{z,1} = C_2 r_1^p, \quad (23)$$

$$H_{\phi,1} = \frac{P}{j\omega\mu r_1} C_2 r_1^p, \quad (24)$$

$$E_{z,N-1} = C_1 r_{N-1}^{-p}, \quad (25)$$

$$H_{\phi,N-1} = -\frac{P}{j\omega\mu r_{N-1}} C_1 r_{N-1}^{-p}. \quad (26)$$

The field components at the boundaries of regions 1 and N still contain unknown constants. The ratios, however, of E_z and H_ϕ at these boundaries contain no constants and it is only these ratios that are needed for a complete solution.

C. Surface impedance calculation

The surface impedance looking outward at a boundary of radius r_n is defined as

$$Z_{n+1} = -\frac{E_{z,n}}{H_{\phi,n}}, \quad (27)$$

and the surface impedance looking inwards is defined as

$$Z_n = \frac{E_{z,n}}{H_{\phi,n}}. \quad (28)$$

With the values of $E_{z,N-1}$, $H_{\phi,N-1}$, $E_{z,1}$, $H_{\phi,1}$ and a_n , b_n , c_n , and d_n as derived in the previous section we have at the current sheet (for $n=g$):

$$Z_{in} = \frac{Z_g \cdot Z_{g+1}}{Z_g + Z_{g+1}}, \quad (29)$$

where Z_{in} is the input surface impedance at the current sheet and Z_{g+1} and Z_g are the surface impedances looking outwards and inwards at the current sheet. Substituting for Z_{g+1} and Z_g using (27) and (28) and rearranging gives

$$Z_{in} = \frac{E_{z,g}}{H_{\phi,g} - H'_{\phi,g}} = -\frac{E_{z,g}}{J'}, \quad (30)$$

thus, the input surface impedance at the current sheet has been determined. This means that all field components can be found by making use of this and (28), (21), (22).

D. The micro-T terminal equivalent circuit

The transmission-line form of (21) and (22) suggests that, by analogy, some form of equivalent circuit is possible [22, 23]. No loss of generality occurs if only one region is considered. The electric and magnetic field quantities are linked as shown in (17). In order to represent the relationship between E_n , H_n and E_{n-1} , H_{n-1} by a corresponding T-circuit, a change of variable refers to the variable H , which is changed to rH . A T-circuit can now be used to link the variables E and rH on either side of a region as shown in Fig. 3.

The current $r_n H_n$ in a T-circuit is driven by a voltage E_n . For the general region n , the impedances are given by the following relations

$$Z_{B,n} = \frac{1}{r_n c_n}, \quad (31)$$

$$Z_{A,n} = Z_{B,n} \left(d_n \frac{r_n}{r_{n-1}} - 1 \right), \quad (32)$$

$$Z_{C,n} = Z_{B,n} (a_n - 1). \quad (33)$$

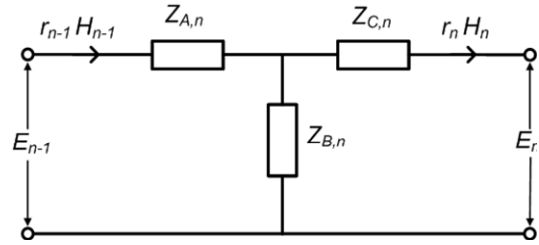


Fig. 3. Basic T-circuit for region n .

When the T-circuits are joined in cascade, the full equivalent circuit is obtained as shown in Fig. 1b where, by the use of (28) and (27), the following expressions are obtained [23].

$$Z_1 = \frac{E_1}{r_1 H_1}. \quad (34)$$

$$Z_N = -\frac{E_{N-1}}{r_{N-1} H_{N-1}}. \quad (35)$$

Thus, an equivalent circuit has been derived by rearrangement of the field solution, where the voltages and currents are directly related to the field quantities. Furthermore, the normal flux density at any interface can be obtained in the form

$$B_{r,n} = \frac{p E_{z,n}}{\omega r_n}. \quad (36)$$

It is convenient to write the equations in terms of phase voltages and currents. The input quantities to the basic equivalent circuit are the current $r_g J'$ and the voltage E_g . The relation between J' and the rms phase current I can be written as

$$r_g J' = \frac{3\sqrt{2} N_{eff} I}{\pi}, \quad (37)$$

where N_{eff} is the effective number of series turns per phase, therefore

$$I = (I_{fac}) J' r_g, \quad (38a)$$

where:

$$I_{fac} = \frac{\pi}{3\sqrt{2} N_{eff}}, \quad (38b)$$

and for a motor of length l m, the rms phase voltage V is related to E_g by

$$V = \sqrt{2} N_{eff} E_g l, \quad (39)$$

therefore,

$$V = (V_{fac})E_g, \quad (40a)$$

where

$$V_{fac} = \sqrt{2}N_{eff}l. \quad (40b)$$

Let us now consider the effect of multiplying the quantities E_n and $r_n H_n$ terms in the basic equivalent circuit by the factors V_{fac} and I_{fac} , respectively; then, the impedances in the basic circuit have to be multiplied by an impedance factor given by

$$Z_{fac} = \frac{V_{fac}}{I_{fac}} = \frac{6N_{eff}^2 l}{\pi}, \quad (41)$$

and the terminal impedance of the machine is given by

$$Z_t = Z_{fac} \frac{Z_{in}}{r_g}. \quad (42)$$

The result is a completely new equivalent circuit in which the input quantities are the rms phase voltage and rms phase current using (40) and (38). Thus, the various voltages and currents at the input to each T-circuit are now related directly to the field quantities at the corresponding interfaces in the machine. The terminal equivalent circuit has all the advantages of the basic circuit but, in addition, the impedances are real impedances. The voltages and currents appearing in the circuit can be used in (40) and (37) in order to obtain the field quantities E_z , B_r , and B_ϕ at any desired region boundary.

Using the terminal impedance, the rotor resistance, rotor leakage reactance, and magnetizing reactance can be obtained.

The rotor resistance is obtained from the terminal impedance at standstill as $r_2 = \text{Re}\{Z_t\}$ and the leakage reactance is obtained from the terminal impedance at standstill as $x_2 = \text{Im}\{Z_t\}$.

The magnetizing impedance is obtained from the terminal impedance at synchronous speed. It should be noted that the real part of the terminal impedance is zero at this speed. The stator winding resistance can be simply joined in series at the input terminals. From above an equivalent circuit analogous to classical theory can be derived as will be shown in the next section.

The time-average input power density P_{in} [W/m²] passing through a surface can be calculated through the concept of the Poynting

theorem in the field solution as:

$$P_{in} = \frac{1}{2} \text{Re}\{\bar{E} \times \bar{H}^*\}, \quad (43)$$

and the total power P_w [W] is given by

$$P_w = \frac{1}{2} |E_g|^2 \text{Re}\left\{\frac{2\pi r_g l}{Z_{in}^*}\right\}. \quad (44)$$

Using the terminal equivalent circuit, the total power is calculated as

$$P_w = 3 \text{Re}\{VI^*\} = 3 \text{Re}\left\{\frac{|V|^2}{Z_t^*}\right\}, \quad (45)$$

and the torque T [N-m] is given by

$$T = \frac{P_w}{\omega}. \quad (46)$$

The force in the circumferential direction F_z is calculated as

$$F_z = \frac{T}{r_r}, \quad (47)$$

where r_r is the outer rotor radius.

IV. NUMERICAL RESULTS

The equivalent circuit method that has been described in the previous section is validated using a commercial finite element program (Comsol Multiphysics [25]) along with a real motor whose data is given in Table I.

Figure 4 shows the finite element discretization of the model. It should be noted that the air gap layer is not visible in this to scale drawing. Figures 5a and 5b show the radial and circumferential flux density components respectively using both the micro-T circuit model and the finite element method (FEM), for standstill and rated speed conditions. The magnitude of flux density is greater at the rated speed since most of the flux is magnetizing while its leakage flux is under standstill conditions.

Figures 6 and 7 show the flux contours at standstill and rated speed, respectively. At the rated speed, the skin depth in the rotor conductor is appreciable, allowing flux to penetrate the rotor core while at a standstill, the skin depth is much lower, hence forcing the flux to concentrate around the air gap.

Table I: Machine data

Rated power, (W)	746
Number of poles	2
Line stator voltage, (V)	220
Number of turns per phase	86
Frequency, (Hz)	60
Rated speed, (rpm)	3358
Efficiency, (%)	89
Rated slip	0.067
Rotor core radius, (mm)	32.6
Outer rotor radius, (mm)	46.5
Inner stator radius, (mm)	46.8
Outer stator radius, (mm)	63
Relative permeability of iron	4000
Rotor conductivity, (S/m)	1.56×10^7

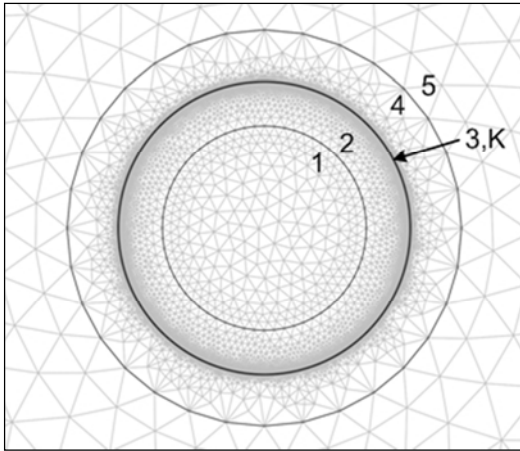


Fig. 4. Finite element discretization of model.

Figure 8 compares the torque-speed characteristic for the following four cases:

- (1) The true behavior of a real motor designed with RMxpert, a commercially available computer software [24], which works based on the magnetic circuit approach to predict the performance parameters. This curve is obtained from the equivalent circuit given by RMxpert and corresponds to the base case.
- (2) The equivalent circuit with the stator resistance neglected. This is done to gauge the effect of the first assumption in the derivation of the analytical model.
- (3) The base case, but with the stator windings

represented by a current sheet and the squirrel cage bars represented by a conductive layer (as in Fig. 4). This case is obtained with finite element simulations using Comsol Multiphysics.

- (4) The plot corresponding to the analytical model of this paper.

One can appreciate that the performance of this paper's model is identical to the numerical solution for the same geometry and not too far from the true motor.

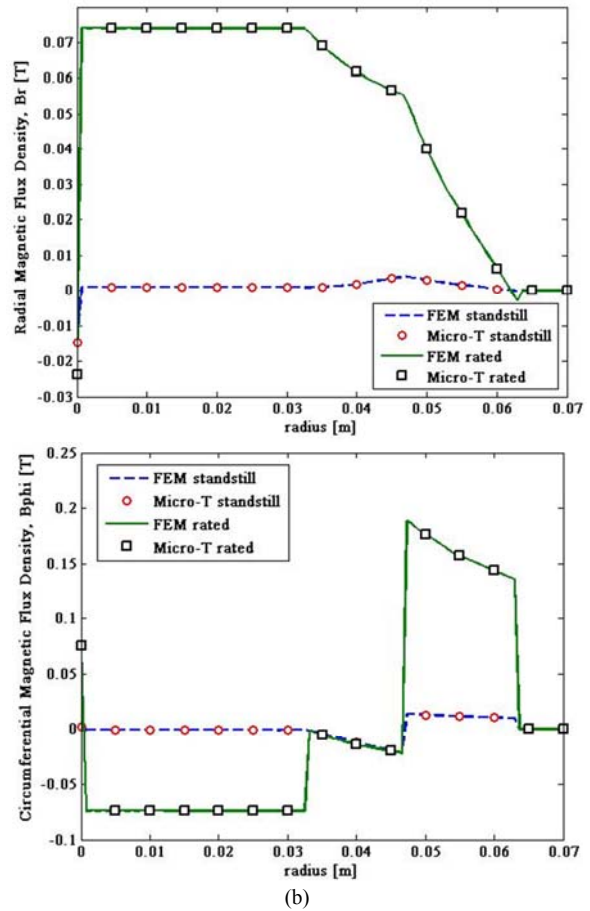


Fig. 5. (a) Comparison of radial flux density computed from FEM and micro-T circuit model. (b) Comparison of circumferential flux density computed from FEM and micro-T circuit model.

V. CONCLUSIONS

The micro-T circuit has been used for the analysis of squirrel-cage induction motors. It can be used for any number of regions, and in addition, with any number of stator poles so that our proposed method of analysis becomes quite general.

Given just the voltages at the terminal equivalent circuit, all field quantities at any region boundary can be easily derived, as well as air gap power, losses, output power and torque.

Using such circuits may provide a better technical insight into the system than is possible from studying the full-wave solutions from a computational electromagnetics analysis.

The obtained results agree well with the data from the corresponding finite element method analysis as well as with the equivalent circuit of a real motor (with no stator). Therefore, the micro-T circuit can reproduce the behavior of the terminal equivalent circuit and gives physical meaning to the elements of the circuit.

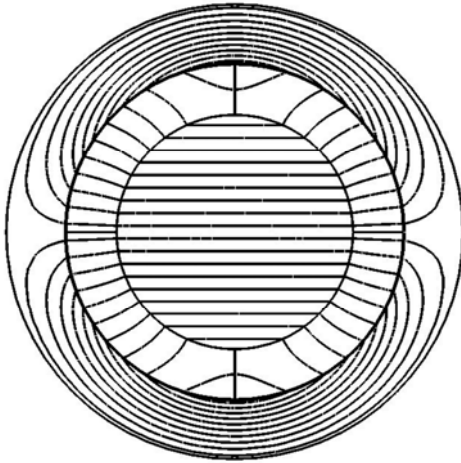


Fig. 6. Flux contour plot at rated speed.

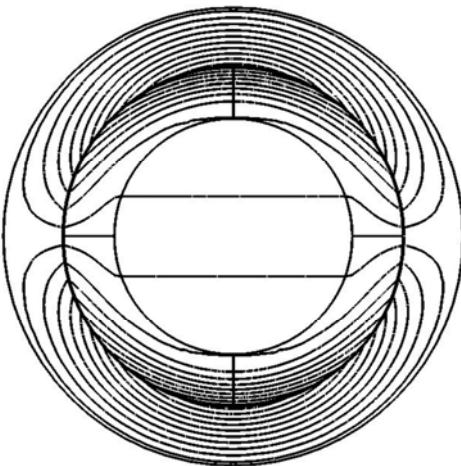


Fig. 7. Flux contour plot at standstill.

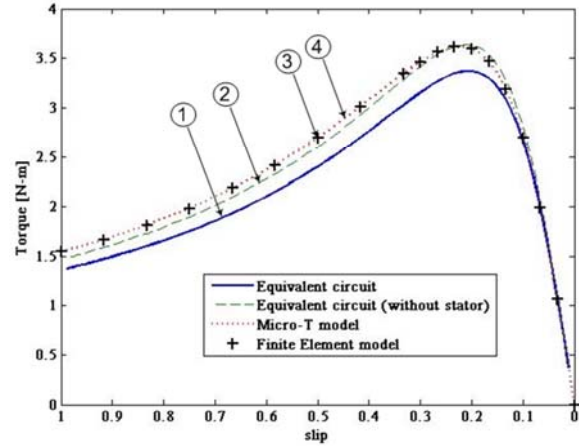


Fig. 8. Comparison of torque-speed characteristics for the following cases: (1) True behavior of the motor computed by RMxpert (reluctance network). (2) Neglecting stator resistance. (3) Stator windings represented as a current sheet and squirrel cage represented by a conductive layer computed with Comsol (FEM). (4) Analytical model of this paper.

VI. APPENDIX – CALCULATION OF THE ELEMENTS OF THE TRANSFER MATRIX

Equations (15) and (16) are solved for the constants C_1 and C_2 at the inner boundary of a non-conducting region n . Then the values of these constants are used for the same region at the outer boundary. The two equations thus obtained relate field quantities at the outer and inner boundary of region n with no constants. The same method is applied for a conducting region whose slip is different from zero using (15) and (16). The result is as follows:

1. Transfer matrix elements for regions in which $s_n \cdot \sigma_n \neq 0$.

$$a_n = -\alpha_n r_{n-1} [I_p(\alpha_n r_n) \cdot K'_p(\alpha_n r_{n-1}) - K_p(\alpha_n r_n) \cdot I'_p(\alpha_n r_{n-1})] \quad (48)$$

$$b_n = -j\omega\mu_n r_{n-1} [I_p(\alpha_n r_{n-1}) \cdot K_p(\alpha_n r_n) - I_p(\alpha_n r_n) \cdot K_p(\alpha_n r_{n-1})] \quad (49)$$

$$c_n = -s_n \sigma_n r_{n-1} [I'_p(\alpha_n r_n) \cdot K'_p(\alpha_n r_{n-1}) - K'_p(\alpha_n r_n) \cdot I'_p(\alpha_n r_{n-1})] \quad (50)$$

$$d_n = -\alpha_n r_{n-1} [I_p(\alpha_n r_{n-1}) \cdot K'_p(\alpha_n r_n) - K_p(\alpha_n r_{n-1}) \cdot I'_p(\alpha_n r_n)] \quad (51)$$

where σ_n and s_n are the conductivity and slip of region n , respectively.

2. Transfer matrix elements for regions in which $s_n \sigma_n = 0$.

$$a_n = \frac{1}{2}(\xi^p + \xi^{-p}), \quad (52)$$

$$b_n = j \frac{1}{2} \omega \mu_n r_{n-1} \left(\frac{\xi^p - \xi^{-p}}{p} \right), \quad (53)$$

$$c_n = \frac{1}{2} \frac{p}{j \omega \mu_n r_n} (\xi^p - \xi^{-p}), \quad (54)$$

$$d_n = \frac{1}{2} \left(\frac{\xi^p + \xi^{-p}}{\xi} \right), \quad (55)$$

where

$$\xi = \frac{r_n}{r_{n-1}}. \quad (56)$$

ACKNOWLEDGEMENT

The authors would like to recognize the contribution of Prof. N. K. Al-Sahib for the support of the University of Baghdad.

REFERENCES

- [1] E. R. Laithwaite, *Induction Machines for Special Purposes*, Newnes, Oxford, U.K., 1966.
- [2] A. L. Cullen and T. H. Barton, "A Simplified Electromagnetic Theory of the Induction Motor using the Concept of Wave Impedance," *Proc. IEE*, vol. 105C, pp. 331-336, 1958.
- [3] L. S. Piggot, "A Theory of the Operation of Cylindrical Induction Motors with Squirrel-Cage Rotors," *Proc. IEE*, vol. 109C, pp. 270-282, 1962.
- [4] E. Mishkin, "Theory of the Squirrel-Cage Induction Motor Derived Directly from Maxwell's Field Equations," *Quart. J. Mech. Appl. Maths.*, no. 7, pp. 472-487, 1954.
- [5] J. C. Wilson, E. A. Erdelyi, and R. E. Hopkins, "Aerospace Composite-Rotor Induction Motors," *IEEE Trans. AES-3*, Suppl., pp. 18-23, 1965.
- [6] J. C. West and D. E. Hesmondhalgh, "The Analysis of Thick-Cylinder Induction Machines," *Proc. IEE*, vol. 109C, pp. 172-181, 1962.
- [7] W. D. Jackson and E. S. Pierson, "Operating Characteristics of the M.P.D. Induction Generator," *IEE conf.*, rep. 4, pp. 38-42, 1962.
- [8] R. L. Stoll and P. Hammond, "Calculation of the Magnetic Field of Rotating Machines-Pt. 4. Approximate Determination of the Field and the Losses Associated with Eddy Currents in Conducting Surfaces," *Proc. IEE*, vol. 112, no. 11, pp. 2083-2094, 1965.
- [9] P. J. Lawrenson, P. Reece, and M. C. Ralph, "Tooth-Ripple Losses in Solid Poles," *Proc. IEE*, vol. 113, no. 4, pp. 657-662, 1966.
- [10] L. Concordia and H. Poritsky, "Synchronous Machine with Cylindrical Rotor," *Trans. Amer. Inst. Elect. Engrs*, vol. 56, pp. 49-58, 1937.
- [11] A. J. Wood, "An Analysis of Solid Rotor Machines," *Trans. Amer. Inst. Elect. Engrs*, vol. 79, pp. 1657-1665, 1960.
- [12] C. Steinmetz, *Theory and Calculation of Alternating Current Phenomena*, W. J. Johnston Company, New York, 1897.
- [13] C. V. Jones, "Unification of Field and Circuit Theories of Electrical Machines," *Proc. IEE*, vol. 119, no. 7, pp. 871-876, 1972.
- [14] B. Beland and J. Richard, "A New Transmission Line Representation of Eddy-Current Problems in Cylinders," *IEEE Trans.* vol. PAS-90, no. 5, pp. 2181-2185, 1971.
- [15] R. Wang and J. M. Jin, "A Symmetric Electromagnetic-Circuit Simulator Based on the Extended Time-Domain Finite Element Method," *IEEE Transactions on Microwave Theory and Techniques*, vol. 56, no. 12, pp. 2875-2884, December 2008.
- [16] M. Feliziani and F. Maradei, "Circuit-Oriented FEM: Solution of Circuit-Field Coupled Problems by Circuit Equations Magnetics," *IEEE Transactions on Magnetics*, pp. 965 - 968, vol. 38, no. 2, Mar. 2002.
- [17] L. J. Qaseer, "The Micro-T Circuit Model for the Analysis of Cylindrical Induction Heating Systems," *IEEE Trans. Energy Convers.*, vol. 25, no. 4, pp. 1021-1027, 2010.
- [18] L. J. Qaseer, "Micro-T Circuit Model for Double and Single Sided Induction Heating Systems," *Applied Computational Electromagnetic Society (ACES) Journal*, vol. 25, no. 8, pp. 713-721, August 2010.

- [19] J. Greig and E. M. Freeman, "Traveling Wave Problem in Electrical Machine," *Proc. IEE*, vol. 114, no. 11, pp. 1681-1683, 1967.
- [20] E. M. Freeman, "Traveling Waves in Induction Machines: Input Impedance and Equivalent Circuits," *Proc. IEE*, vol. 115, no. 12, pp. 1772-1776, 1968.
- [21] E. M. Freeman and B. E. Smith, "Surface Impedance Method Applied to Multilayer Cylindrical Induction Devices with Circumferential Exciting Currents," *Proc. IEE*, vol. 117, no. 10, pp. 2012-2013, 1970.
- [22] L. A. Pipes, "Matrix Theory of Skin Effect in Laminations," *J. Franklin Inst.*, vol. 262, pp. 127-138, 1956.
- [23] E. M. Freeman and T. G. Bland, "Equivalent Circuit of Concentric Cylindrical Conductors in an Axial Alternating Magnetic Field," *Proc. IEE*, vol. 123, no. 2, pp. 149-152, 1976.
- [24] Ansoft RMxprt,
<http://www.ansoft.com/products/em/rmxprt/>
- [25] Comsol Multiphysics, *ACDC Module User's Guide*, Comsol AB Group, 2010, pp. 1-222.



Layth Qaseer received his B.Sc., M.Sc., and Ph.D. degrees from the University of Baghdad, Baghdad, Iraq in 1979, 1993, and 2004 respectively, all in electrical engineering. Between 1979 and 2001, he worked at the National Scientific Research Center and the Ministry of Industry. In 2005, he joined the Department of Mechatronic Engineering at the University of Baghdad. He is currently with the Department of Electrical and Computer Engineering at the Polytechnic Institute of New York University. His research interest includes rotary, flat linear, tubular linear, and helical motion induction motors as well as induction heating systems.



Francisco de León (S'86–M'92–SM'02) received the B.Sc. and the M.Sc. (Hons.) degrees in Electrical Engineering from the National Polytechnic Institute, Mexico City, Mexico, in 1983 and 1986, respectively, and the Ph.D. degree from the University of Toronto, Toronto, ON, Canada, in 1992. He has held several academic positions in Mexico and has worked for the Canadian electric industry. Currently, he is an Associate Professor at the Polytechnic Institute of NYU, Brooklyn, NY. His research interests include the analysis of power definitions under nonsinusoidal conditions, the transient and steady-state analyses of power systems, the thermal rating of cables and transformers, and the calculation of electromagnetic fields applied to machine design and modeling.



Sujit Purushothaman (S'09) received his B.E. degree in Electrical Engineering from Mumbai University (Sardar Patel College of Engineering), India in 2005. His work experience includes testing and development of medium voltage switchgear for Siemens India. He received his Master's degree in 2009 and is currently pursuing his Ph.D. at Polytechnic Institute of NYU. His research interest includes power system transients, subsynchronous resonance damping, machine design and modeling, and thermal modeling of electrical machines.